The Journal of Green Energy and Environmental Engineering

Research Paper

Preparation and Antibacterial Properties of Cellulose Nanofibrils/ Nanocarbon Composites

Truman Capote [1], Harper Lee [2,*]

[1] Laboratory of Catalysis and Catalytic Processes, Dipartimento di Energia, Politecnico di Milano, via La Masa 34, Milano, 20156, Italy
[2] FibRe Centre for Lignocellulose-based Thermoplastics, Chalmers University of Technology, Gothenburg, Sweden
*Corresponding author: Truman.Capote@usp.br; Lee369@psu.edu

Abstract. Cellulose nanofibrils (CNFs) were prepared from waste cut tobacco via an ionic-liquid-assisted ball-milling method. The as-obtained CNFs were compounded with nanocarbon particles (CNPs) by ultrasonic treatment to yield CNFs/CNPs composites, which were further blended with polyvinyl alcohol (PVA) to fabricate CNFs/CNPs/PVA composite films. The samples were characterized by SEM, FTIR, TGA, DSC and XRD; their rheological behaviors and particle sizes were measured, and the antibacterial activity of CNFs/CNPs/PVA films was evaluated. The results show that compared with pure CNFs, CNFs/CNPs composites possess smoother surfaces with fewer filament-like structures and more granular particles. The particle sizes of CNFs are mainly distributed in the range of 340-540 nm. Aqueous suspensions of CNFs/CNPs composites exhibit shear-thinning behavior at shear rates higher than 0.2 s^{-1}. Both CNFs and CNFs/CNPs composites retain the cellulose-I crystal structure. The crystallinity of CNFs/CNPs composites rises from 35.40 % (pure CNFs) to 45.38 %. The temperature corresponding to the maximum thermal degradation rate increases from 361.33 °C for CNFs to 376.40 °C for CNFs/CNPs composites. CNFs/CNPs/PVA films display antibacterial effects against *Staphylococcus aureus*, *Escherichia coli* and *Salmonella*, whereas no obvious inhibitory effect is observed for *Bacillus subtilis*. The antibacterial rates of CNFs/CNPs composites against *Escherichia coli* and *Staphylococcus aureus* reach 93.92 % and 95.04 %, respectively. The antibacterial performance of CNFs/CNPs composites is primarily contributed by CNPs. The antibacterial mechanism originates mainly from negative charges on CNPs surfaces, which adsorb bacteria and consequently induce bacterial death.

Keywords: *cellulose nanofibrils; nanocarbon; composites; antibacterial properties; functional materials*

Received on 02 July 2025, Accepted on 05 Nov 2025, Published on 15 Dec 2025

1 Introduction

China is a major tobacco-producing country. Large quantities of tobacco waste are generated during tobacco production and processing[1]. At present, domestic research on tobacco waste mainly focuses on fertilizer production, extraction of effective chemical constituents and substrate-oriented material applications[2-3]. Tian Junling et al.[4] reported applications of tobacco waste in fertilizers, including direct utilization, utilization after compost fermentation, and compost fermentation after compound extraction. Efficient and rational utilization of tobacco waste remains one of the key challenges for the tobacco industry.

The mass fraction of cellulose in tobacco leaves is approximately 11 %[5], and an even higher content is found in tobacco stems. Cellulose consists of amorphous and crystalline regions. Different processing routes can produce various forms of nanocellulose. Over the past few years, nanocellulose has drawn widespread interest

thanks to its large aspect ratio, remarkable mechanical properties, and its renewable and biocompatible nature[6-7]. Depending on its source and morphology, nanocellulose is generally grouped into three categories: cellulose nanocrystals (CNCs)[8], cellulose nanofibrils (CNFs)[9], and bacterial nanocellulose (BNC)[10-11]. CNFs feature high hydrophilicity, excellent mechanical properties and favorable biodegradability[12], and have high research value for composite-material development. Main preparation methods for CNFs include mechanical and chemo-mechanical approaches[13]. Mechanical methods cover high-pressure homogenization, ultrasonic treatment, ball-milling and cryogenic crushing. Ball-milling is usually combined with chemical pretreatment. Adding ionic-liquid solvents during ball-milling disrupts intra- and intermolecular hydrogen bonds of cellulose and induces cellulose swelling. Bao Hanxiao et al.[14] prepared CNFs from pineapple peel residues using NaOH solution combined with mechanical ball-milling. Their results indicated that increasing NaOH concentration lowered CNF yield while improving crystallinity. Meng Fanjie et al.[15] fabricated nanocellulose/carbon nanofiber composite membranes by electrospinning and found that the incorporation of nanocellulose enhanced hydrophobicity. Nanocellulose possesses excellent mechanical performance, biocompatibility, biodegradability and film-forming capacity. Zhang Fan et al.[16] introduced nanocellulose as a carrier for inorganic antibacterial nanoparticles, which represents an important research direction for nanocellulose-based antibacterial composites. Polyvinyl alcohol (PVA) is one of the most widely used non-toxic biodegradable polymers in food packaging, featuring superior film-forming ability, biocompatibility and oxygen-barrier performance[17]. Ma Jiabo et al.[18] prepared lemon peel/PVA/bacterial-cellulose composite films and investigated their antibacterial activity, demonstrating that composite films containing lemon peel exhibited strong bacterial inhibition. Kang Xingya et al.[19] manufactured nano-ZnO/CNCs/PVA composite films via ultrasonic mixing. The addition of CNCs improved mechanical and moisture-barrier properties of PVA films, while nano-ZnO endowed the composite films with certain inhibitory activity against *Staphylococcus aureus*.

In this work, waste cut tobacco was adopted as raw material. Cellulose was first extracted from waste cut tobacco by alkaline-oxidative treatment, followed by ionic-liquid treatment and ball-milling to obtain CNFs. CNFs were assembled with nanocarbon particles (CNPs) under ultrasonication to produce CNFs/CNPs composites. The samples were characterized and analyzed by SEM, XRD, FTIR, simultaneous thermal analysis and rotational rheometry. Using CNFs/CNPs composites together with PVA as the matrix, composite films were fabricated and subsequently tested for antibacterial activity. This study aims to provide references for expanding the application scope of CNFs/CNPs composites in antibacterial fields.

2 Experimental Section

2.1 Materials, Reagents and Instruments

China Tobacco Shaanxi Industrial Co., Ltd. provided the waste cut tobacco used in this work. The test microorganisms — Escherichia coli (CMCC 44102), Staphylococcus aureus (CMCC 26003), and Bacillus subtilis (ATCC 6633) — were obtained from Beijing Biobw Biotechnology Co., Ltd. *Salmonella* (BNCC 103134) obtained from Beijing Beina Chuanglian Biotechnology Research Institute.

Reagents: Sodium hydroxide (NaOH, Yantai Shuangshuang Chemical Co., Ltd.); hydrogen peroxide H2O2, mass fraction 30 %, Sinopharm Chemical Reagent Co., Ltd.); CNPs (purity > 95 %, particle size 10-70 nm, Beijing Sinna Advanced Materials Co., Ltd.); 1-butyl-3-methylimidazolium chloride ([BMIM]Cl), polyvinyl alcohol (PVA, relative molecular mass \(6.7\times10^{4}\)), Shanghai Macklin Biochemical Co., Ltd.; yeast extract, peptone (Thermo Fisher Scientific); sodium chloride (Tianjin Fengchuan Chemical Reagent Science-Technology Co., Ltd.); agar powder (Beijing Solarbio Science-Technology Co., Ltd.). All reagents were of analytical grade.

Instruments: 5810R high-speed refrigerated centrifuge (Eppendorf, Germany); YXQ-70A vertical pressure steam sterilizer (Shanghai Boxun Medical Biological Instrument Co., Ltd.); SW-CJ-1F clean bench (Suzhou Antai Air-tech Co., Ltd.); Zetasizer Nano ZS90 particle size & zeta-potential analyzer (Malvern, UK); D8 Advance X-ray diffractometer (XRD), Vertex 70 Fourier-transform infrared spectrometer (FTIR) (Bruker, Germany); STA449F3 simultaneous thermal analyzer (TGA-DSC) (Netzsch, Germany); JSM-7001F field-emission scanning electron microscope (SEM) (JEOL, Japan); Discovery HR-1 rotational rheometer (TA Instruments, USA).

2.2 Experimental Methods

2.2.1 Extraction of Cellulose

The dried cut tobacco was first ground into a fine powder with a mechanical grinder. A 30.0 g portion of this powder was then dispersed in 600 mL of 4 wt% NaOH solution, corresponding to a solid-to-liquid ratio of 1∶20 (g∶mL), and the dispersion was refluxed at 90 °C for 100 min. Once the system had cooled to 70 °C, a 5 wt% H_2O_2 solution was introduced and allowed to react for a further 30 min. Solids were subsequently recovered by centrifuging the suspension at 5000 r/min for 15 min, after which four cycles of washing with deionized water and re-centrifugation afforded the product as a yellow mixed suspension. Finally, cellulose solid was obtained by freeze-drying at −56 °C for 48 h.

2.2.2 Preparation of CNFs

An aqueous [BMIM]Cl solution at a concentration of 30 wt% was first prepared. Cellulose was then combined with this solution in a ball mill at a solid-to-liquid ratio of 1∶10, and milling was conducted at an operating frequency of 50 Hz for 1200 s per cycle, with 300 s pauses between runs, repeated over four cycles in total. The milled suspension was centrifuged at 8000 r/min for 15 min, and the recovered solid was redispersed in deionized water, with this washing–centrifugation step repeated four times. Purification was completed by transferring the suspension into dialysis bags (3.5 kDa molecular-weight cutoff) and dialyzing for 48 h, after which freeze-drying at −56 °C for 48 h yielded the CNFs.

2.2.3 Preparation of Composites

CNFs and CNPs were blended with deionized water in a proportion of 2∶1∶400 (g∶g∶mL), using 1.0 g of CNFs, until a uniform mixture was obtained. This mixture was sonicated for 1 h and then spun at 8000 r/min for 10 min; the collected solid underwent four successive rounds of rinsing with deionized water followed by centrifugation. CNFs/CNPs composites were obtained by freeze-drying at −56 °C for 48 h.

2.2.4 Preparation of Films

Films were fabricated according to the protocol described in reference [20]. Specifically, 21.6 g of PVA was dissolved in 540 mL of deionized water with continuous stirring at 90 °C. Once the solution had returned to room temperature, glycerol at 0.65 wt% and CNFs at 0.02 wt% were introduced in sequence, and the blend was sonicated for 1 h to ensure uniform dispersion. A 90 mL aliquot of the resulting solution was then poured into a polytetrafluoroethylene mold (17 cm in outer dimension, 15 cm inner dimension, 1 cm deep) and dried at 60 °C for 3–4 h, yielding the CNFs/PVA composite films.

Following the identical procedure for CNFs/PVA films while replacing CNFs with CNFs/CNPs composites, CNFs/CNPs/PVA films were prepared. Pure PVA films were manufactured by the same protocol without adding CNFs.

2.3 Characterization and Performance Tests

2.3.1 Characterization Methods

For SEM examination, the specimens were first coated with a sputtered gold layer and then imaged in low-energy secondary-electron (LEI) mode at an operating current of 20 μA and an accelerating voltage of 5.0 kV.

Particle-size measurement: Appropriate CNFs sample was dispersed in deionized water, ultrasonicated for 30 min. Three parallel scans were performed at room temperature on the particle-size analyzer; arithmetic mean values were reported.

FTIR measurement: KBr pellet method, wavenumber range 4000-400 cm^{-1}, resolution 4 cm^{-1}, 32 scanning cycles.

TGA-DSC measurement: Nitrogen atmosphere, gas flow 20 mL/min, temperature 28-700 °C, heating rate 10 °C/min.

XRD measurement: Cu target, tube voltage 40 kV, tube current 40 mA, wavelength 0.1541 nm, scanning rate 8 (°)/min, scanning range 0°-80°.

2.3.2 Performance Tests

2.3.2.1 Rheological Behavior Test

Steady-state rheological tests were carried out for aqueous suspensions of CNFs and CNFs/CNPs composites (solid content 0.72 %). 1.5 mL suspension was measured with a 25 mm fixture; shear-rate range \(1*10-1-1*103, test temperature 25 °C.

2.3.2.2 Antibacterial-Activity Test

Suspensions of E. coli, S. aureus, Salmonella, and B. subtilis were adjusted to a cell density of $1*10^6$ CFU/mL, and 100 µL of each was spread over LB agar medium (composed of 10 g/L peptone, 5 g/L yeast extract, 10 g/L NaCl, and 20 g/L agar). The films were punched into 6 mm discs and disinfected under UV light for 30 min; then, working in a clean bench, the discs were laid on the inoculated agar surfaces. After sealing, the plates were kept in a biochemical incubator at 37 °C for 24 h before bacterial growth was examined[21].

The plate-counting method was used to evaluate composite antibacterial capacity. Activated *E. coli* and *S. aureus*suspensions were diluted to $1*10^6$ CFU/mL. 1 mL bacterial suspension was mixed separately with 1 mL physiological saline (blank control CK), 1 g/L CNFs suspension and 1 g/L CNFs/CNPs composite suspension in 10-mL shake tubes. Samples were incubated in a shaker at 37 °C, 200 r/min for 60 min. Treated bacterial suspensions were serially diluted by $1*10^6$. 100 µL diluted suspension was spread evenly on LB agar medium, incubated upside-down at 35 °C for 24 h. Colony numbers Nm on plates were counted. N0 denotes colony count of the blank saline control group.

3 Results and Discussion

3.1 Sample Characterization

3.1.1 SEM Analysis

Figure 1 presents SEM micrographs of CNPs, CNFs and CNFs/CNPs composites.

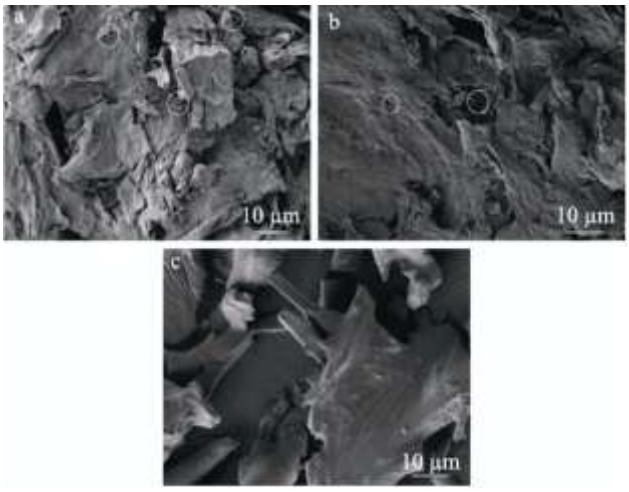

Figure 1 SEM images: (a) CNFs; (b) CNFs/CNPs composites; (c) CNPs

3.1.2 Particle-Size Distribution Analysis

Figure 2 shows particle-size distribution of CNFs.

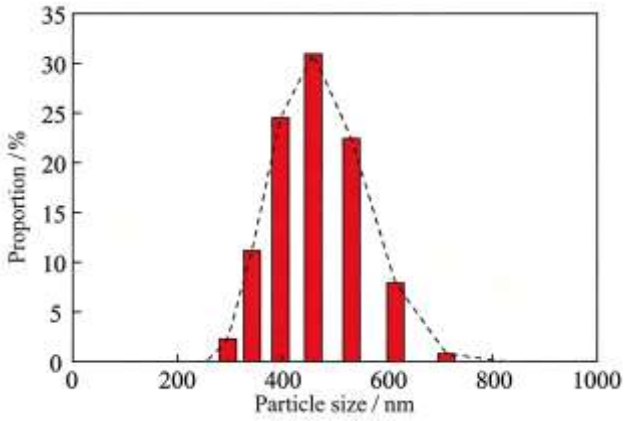

Figure 2 Particle-size-distribution diagram of CNFs

The fraction of CNFs particles with sizes between 340-540 nm reaches 89 %. Particle sizes are relatively concentrated and uniformly distributed. Compared with CNFs prepared from lemon-seed raw materials reported in literature[26] 577.28 nm, the CNFs prepared in this work possess smaller average particle size.

3.1.3 XRD Analysis

Figure 3 displays XRD patterns of CNPs, CNFs and CNFs/CNPs composites.

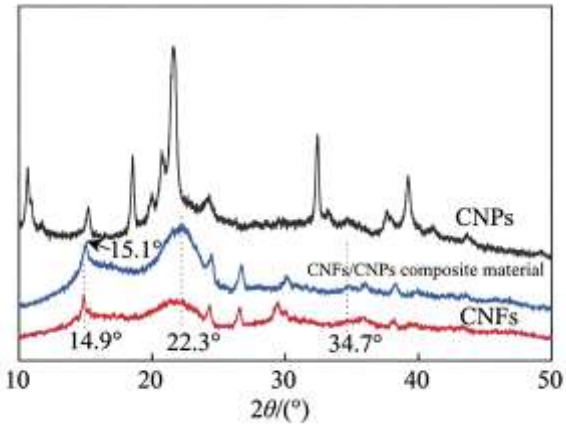

Figure 3 XRD patterns of CNFs, CNPs and CNFs/CNPs composites

Both CNFs and CNFs/CNPs composites exhibit three main diffraction peaks at 2theta=14.9o, 22.3 o and 34.7 o, corresponding to the (1-10), (200) and (004) crystal planes of cellulose-I, which agrees with published results[27-28]. This demonstrates that the original cellulose crystal form is preserved throughout CNFs preparation and ultrasonic compounding with CNPs. CNPs show stronger diffraction-peak intensities. After compounding, diffraction-peak intensities of CNFs are enhanced without peak-position shifts, proving physical combination between CNFs and CNPs. Characteristic diffraction peaks of CNPs are absent in composite patterns, which may be attributed to low relative content of CNPs or peak overlap by CNFs diffraction signals[29].

Calculated from Figure 3 using Equation 1 and 2, the crystallinity index of CNFs/CNPs composites (45.38 %) is distinctly higher than that of CNFs (35.40 %). Hydrogen-bond formation between CNFs and CNPs contributes to

increased crystallinity. The crystallinity of as-prepared CNFs is lower than that of lemon-seed-derived CNFs (54.78 %) reported in reference [26], which is ascribed to differences in ball-milling duration and ionic-liquid dosage during preparation.

3.1.4 FTIR Analysis

Figure 4 shows FTIR spectra of CNPs, CNFs and CNFs/CNPs composites.

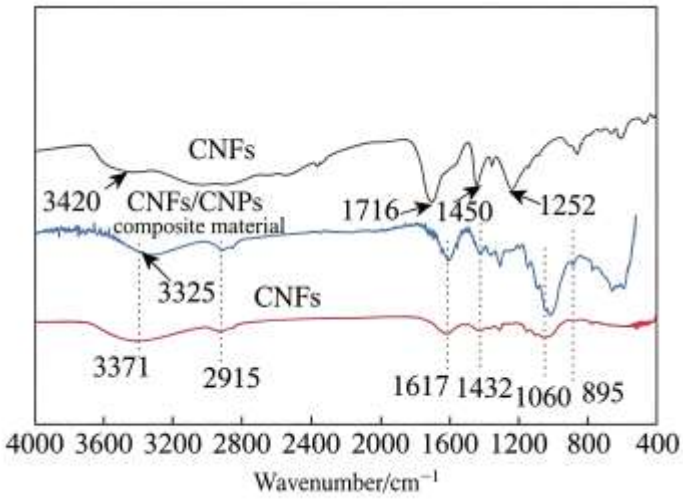

Figure 4 FTIR spectra of CNFs, CNPs and CNFs/CNPs composites

The CNPs display high overall spectral transmittance. In their spectrum, the broad absorption near 3420 cm^{-1} arises from –OH stretching, the signal at 1716 cm^{-1} reflects the C=O stretching of carboxyl moieties, the feature at 1450 cm^{-1} is due to in-plane C–H bending, and the band at 1252 cm^{-1} stems from asymmetric C–O–C stretching — collectively verifying the presence of both carboxyl and hydroxyl functionalities in the CNPs.

Characteristic peaks of CNFs and CNFs/CNPs composites appear at 3371, 2915, 1617, 1432, 1060 and 895 cm-1, matching typical absorption-band positions of cellulose-I in literature[28,30]. It indicates that the fundamental chemical structure of cellulose remains intact during CNFs fabrication and composite synthesis. The spectrum exhibits a wide –OH stretching envelope spanning 3800–3300 cm^{-1}, while the sharp signal at 2915 cm^{-1} arises from C–H stretching within $–CH_2–$ groups. The feature at 1617 cm^{-1} is attributed to the bending of hydroxyl groups associated with adsorbed water, that at 1432 cm^{-1} to $–CH_2–$ bending, and that at 1060 cm^{-1} to C–O stretching. In addition, the band at 895 cm^{-1} originates from C–H vibrations linked to the β-glycosidic connections between glucose units in the cellulose backbone[31]. After compounding CNFs with CNPs, the 3371 cm-1 band shifts toward lower wavenumbers (red shift) accompanied by intensity enhancement. No new chemical-bond signals emerge. Carboxyl and hydroxyl groups on CNPs readily form intermolecular hydrogen bonds with abundant hydroxyl sites on CNFs, accounting for the red-shift phenomenon of hydroxyl stretching bands in composites.

3.1.5 TGA-DSC Analysis

Figure 5 presents TGA and DSC curves for CNPs, CNFs and CNFs/CNPs composites. Table 1 summarizes major pyrolysis parameters of CNFs and CNFs/CNPs composites.

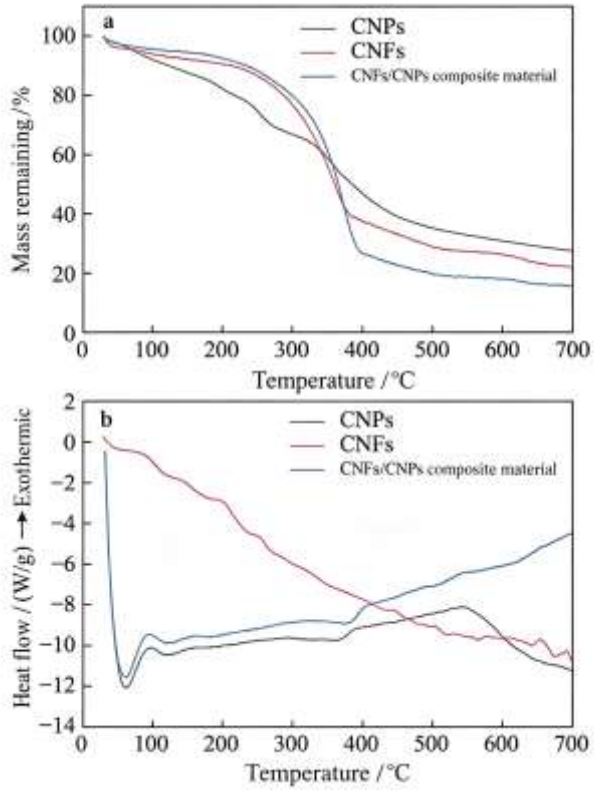

Figure 5 (a) TGA curves; (b) DSC curves of CNFs, CNPs and CNFs/CNPs composites

Table 1 Main pyrolysis parameters of CNFs and CNFs/CNPs composites

Sample	Onset degradation temperature / °C	Temperature at maximum thermal-degradation rate / °C	Residual carbon / %
CNFs	300.56	361.33	21.77
CNFs/CNPs composites	320.24	376.40	15.48

As illustrated in Figure 5a, thermal-weight-loss processes of CNFs and CNFs/CNPs composites can be divided into three stages. Stage 1 (30-240 °C): slow mass loss caused by evaporation of adsorbed or bound water[32]. Stage 2 (240-390 °C): drastic weight loss, corresponding to degradation of CNFs and decomposition of glucose units. Massive bond cleavage of C-O and C-C bonds takes place, generating gaseous products (\(CO_{2}\), \(H_{2}O\), CO) and carbonized residues[31]. Stage 3 (390-700 °C): weight loss originates from further oxidative decomposition of carbonized products into low-molecular-weight gaseous species[33]. For CNPs, weight loss below 220 °C mainly comes from water evaporation; oxidation and pyrolysis reactions proceed upon further heating, leading to continuous mass reduction.

From DSC curves (Figure 5b), the glass-transition region for CNFs and CNFs/CNPs composites lies within 30-80 °C, with glass-transition events observable near 65 °C. Endothermic peaks at 100-150 °C correspond to water evaporation; endothermic peaks at 350-400 °C are associated with molecular-chain scission. The peak temperature of CNFs/CNPs composites (≈380 °C) is higher than that of pure CNFs (≈370 °C), consistent with TGA results. The DSC curve of CNPs keeps descending: water evaporation absorbs heat at low temperature and lowers heat-release rate; as temperature rises, oxidation and pyrolysis of CNPs accelerate, gradually increasing heat-release rate.

According to Table 1, the temperature at maximum thermal-degradation rate for CNFs/CNPs composites reaches 376.40 °C, higher than 361.33 °C of CNFs. The main pyrolysis peak shifts toward higher-temperature zones, confirming improved thermal stability for composites, which can be explained by strong hydrogen-bond interactions formed between CNFs and CNPs[12]. Both samples show maximum thermal-degradation-rate temperatures higher than approximately 350 °C reported for nanocellulose in reference [34].

3.2 Rheological-Behavior Analysis

Figure 6 displays shear-stress-shear-rate and viscosity-shear-rate curves for CNPs, CNFs and CNFs/CNPs composites.

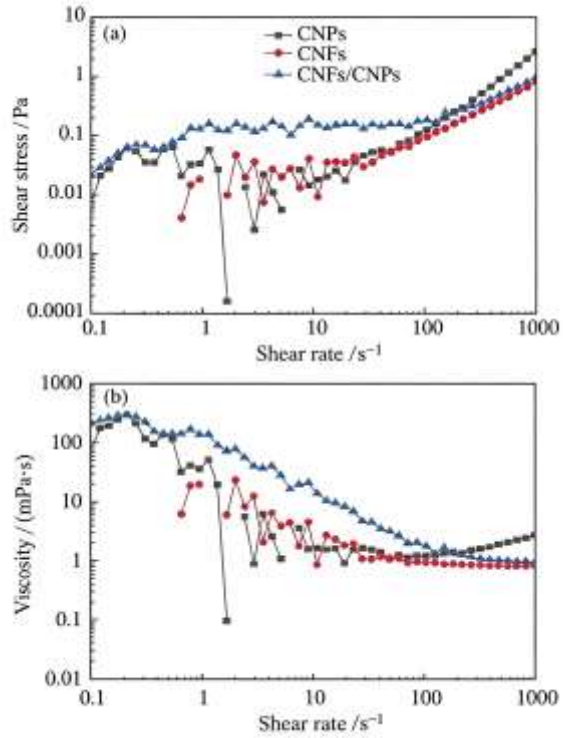

Figure 6 (a) Shear-stress vs shear-rate curves; (b) viscosity vs shear-rate curves for CNPs, CNFs and CNFs/CNPs composites

As shown in Figure 6a, shear stress increases with rising shear rate for all three materials, and the curves deviate from linear relationships[35]. As seen in Figure 6b, both the CNPs and the CNFs/CNPs composite systems respond as Newtonian fluids when the shear rate remains under 0.2 s^{-1}. Beyond this threshold, however, the composite dispersions become progressively less viscous as the shear rate rises — a shear-thinning response typical of pseudoplastic fluids[36-37]. Shear stress breaks hydrogen-bond interactions among CNF-CNF, CNF-CNPs and CNF-water molecules, reducing viscosity and inducing shear-thinning phenomena[38].

At low shear-rate conditions, CNFs/CNPs composites possess higher viscosity compared with pure CNFs and CNPs, implying better anti-sedimentation performance, water resistance, anti-sagging property and storage stability[39].

3.3 Antibacterial-Activity Analysis

Figure 7 presents inhibition-zone photographs of pure PVA films, CNFs/PVA films and CNFs/CNPs/PVA films against *E. coli*, *S. aureus*, *Salmonella* and *B. subtilis*.

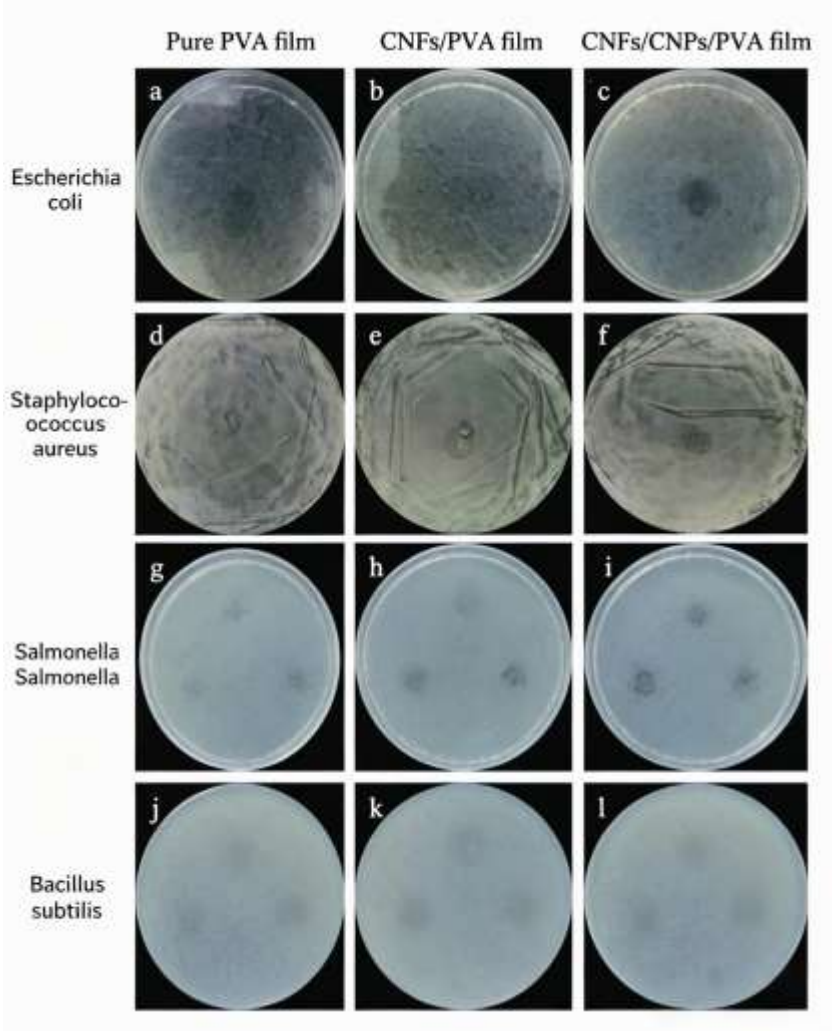

Figure 7 Photographs of antibacterial inhibition zones for pure PVA film, CNFs/PVA film and CNFs/CNPs/PVA film

Neither the neat PVA film nor the CNFs/PVA film shows any detectable activity against S. aureus or E. coli. In contrast, clear growth inhibition of S. aureus, E. coli, and Salmonella is observed for the CNFs/CNPs/PVA films, although these films remain essentially ineffective against B. subtilis. Owing to high water-absorbing capacity of PVA, pure PVA films dissolve and spread outward upon contact with agar medium, resulting in merging between film and medium as observed in photographs. Physical and chemical membrane disruption represents one major antibacterial mechanism for nanomaterials[40-41]. The favorable antibacterial performance of CNFs/CNPs/PVA films arises from negative charges on CNPs surfaces: CNPs adsorb bacterial cells and trigger bacterial death[42-43].

Figure 8 shows antibacterial test photographs for CNFs and CNFs/CNPs composites. CNFs slightly promote bacterial proliferation, whereas CNFs/CNPs composites deliver excellent bacteriostatic performance. Plate-count assays indicate that the composite suppresses the proliferation of S. aureus and E. coli, reaching antibacterial efficiencies of 95.04% and 93.92%, respectively. It proves that CNPs dominate the antibacterial function within CNFs/CNPs composites.

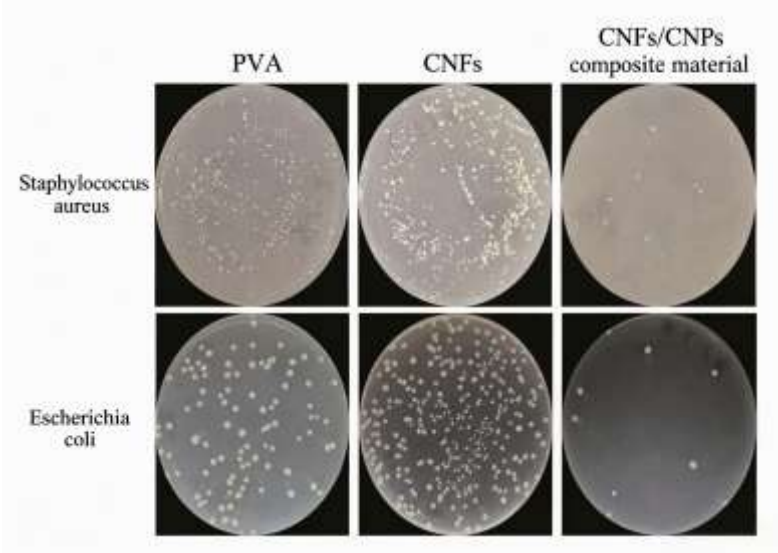

Figure 8 Antibacterial-effect photographs of CNFs and CNFs/CNPs composites

In this study, cellulose nanofibrils (CNFs) were extracted from waste cut-tobacco via alkaline-oxidative pretreatment combined with ionic-liquid-assisted ball-milling. Ultrasonic mixing was adopted to assemble CNFs with nanocarbon particles (CNPs), yielding CNFs/CNPs composites, which were further blended with polyvinyl alcohol (PVA) to fabricate functional composite films. Improved thermal stability and antibacterial performance are mainly driven by intermolecular hydrogen-bond interactions between CNFs and CNPs, as well as the intrinsic surface properties of nanocarbon particles.

The prepared pure CNFs retain the native cellulose-I crystal structure, yet they feature relatively low crystallinity (35.40 %), abundant surface voids and exposed filament-like fibrous textures. After introducing CNPs under ultrasonic treatment, carboxyl and hydroxyl groups distributed on CNPs surfaces form extensive intermolecular hydrogen bonds with plentiful hydroxyl groups on CNF chains. FTIR spectra confirm this interaction through the red-shift of hydroxyl stretching bands, while no new covalent-bond characteristic peaks appear, demonstrating that CNFs and CNPs are combined by physical hydrogen-bond cross-linking rather than chemical covalent reaction. Such hydrogen-bond networks reorganize the stacking of cellulose molecular chains, eliminating partial amorphous regions and increasing composite crystallinity up to 45.38 %. Microscopically, CNPs are uniformly anchored onto CNF substrates, smoothing surface textures and reducing void and fibrous features, which proves good interfacial compatibility between the two phases.

The reinforced hydrogen-bond network accounts for distinctly enhanced thermal stability. For pure CNFs, the maximum thermal-degradation rate occurs at 361.33 °C. In CNFs/CNPs composites, tight hydrogen-bonding restricts molecular-chain mobility and postpones bond cleavage during heating. Consequently, the onset degradation temperature rises from 300.56 °C to 320.24 °C, and the peak temperature of maximum thermal-degradation rate shifts to 376.40 °C. In rheological aspects, the hydrogen-bond-connected composite network raises low-shear viscosity of aqueous suspensions. When shear rates exceed 0.2 s^{-1}, external shear force breaks transient hydrogen-bond junctions, producing typical shear-thinning pseudoplastic fluid behaviour. Higher low-rate viscosity also improves suspension storage stability and anti-sedimentation capacity for subsequent film-forming processing.

Most notably, CNPs endow the composite system with prominent antibacterial capacity, whereas pure CNFs show negligible or even slightly bacteria-promoting effects. Negatively-charged functional groups on CNPs surfaces constitute the core antibacterial origin. When bacterial cells contact composite materials, electrostatic attraction drives CNPs to adsorb bacterial cells. This surface interaction disturbs bacterial surface states and further triggers bacterial death. Experimental results show CNFs/CNPs composites achieve 93.92 % and 95.04 % antibacterial rates against Escherichia coli and Staphylococcus aureus, respectively. The corresponding CNFs/CNPs/PVA composite films exert obvious inhibitory effects on E. coli, S. aureus and Salmonella, yet fail to

suppress Bacillus subtilis, which may relate to the special cell-wall structure of gram-positive spore-forming bacteria.

Nevertheless, the original cellulose-I crystal framework remains intact after compounding, indicating that CNPs function as a functional filler without destroying the fundamental crystalline skeleton of tobacco-derived CNFs. In summary, hydrogen-bond-mediated physical assembly between CNFs and CNPs optimizes crystallinity and thermal resistance, and negatively-charged CNPs provide effective bactericidal activity. This work realizes high-value recycling of tobacco waste and provides feasible design ideas for biomass-based antibacterial composite films applied in packaging and medical-related fields.

Table 2 Performance Comparison of CNFs/CNPs Composites with Reported Biomass-Derived Antibacterial Materials

Material	Raw Source	Preparation	Particle Size	CI	T_{max} (°C)	Antibacterial Performance	Key Feature / Ref.
CNFs (this work)	Waste cut tobacco	Alkaline-H_2O_2 pretreatment + [BMIM]Cl-assisted ball milling	340–540 nm (89%)	35.40%	361.33	Negligible; slightly promotes bacterial growth	Tobacco-waste valorization; low crystallinity due to ball-milling intensity
CNFs/CNPs (this work)	Tobacco CNFs + nanocarbon particles (10–70 nm)	Ultrasonic self-assembly (CNF:CNP = 2:1)	—	45.38%	376.40	*E. coli*93.92%; *S. aureus*95.04%	H-bond-driven physical assembly; CNPs dominate antibacterial activity via surface negative charges
CNFs/CNPs/PVA film (this work)	CNFs/CNPs + PVA (0.02 wt% filler)	Solution casting (60 °C)	—	—	—	Active against *E. coli*, *S. aureus*, *Salmonella*; inactive against *B. subtilis*	Biodegradable packaging/medical film; PVA matrix preserves CNPs bactericidal function
Lemon-seed CNFs	Lemon seeds	Ionic-liquid-assisted ball milling	577.28 nm	54.78%	—	Not tested	Higher crystallinity; larger particle size than tobacco CNFs [26]
Pineapple-peel CNFs	Pineapple peel	Dilute NaOH + mechanical ball milling	—	—	—	Not tested	NaOH concentration inversely affects yield, positively affects crystallinity [14]
Nano-ZnO/CNCs/PVA film	CNCs + nano-ZnO + PVA	Ultrasonic mixing	—	—	—	Moderate inhibition against *S. aureus*	ZnO provides antibacterial function; CNCs improve mechanical & moisture barrier [19]
Lemon peel/PVA/bacterial cellulose film	Lemon peel extract + bacterial cellulose + PVA	Solution blending	—	—	—	Strong antibacterial activity (lemon peel bioactive compounds)	Natural extract-based; no inorganic nanoparticles [18]
PVA/g-C_3N_4 nanofiber membrane	PVA + graphitic carbon nitride	Electrospinning	—	—	—	Visible-light-activated bacteriostasis	Photodynamic mechanism; requires light irradiation [21]
General nanocellulose (literature baseline)	Various biomass	Multiple routes	—	—	~350	None (intrinsically non-antibacterial)	Reference thermal-stability benchmark [34]

4 Conclusions

CNFs were prepared from waste cut-tobacco raw material, and further compounded with CNPs to produce CNFs/CNPs composites.

Physical ball-milling and chemical alkaline pretreatment do not alter the crystal form of CNFs and CNFs/CNPs composites; both retain cellulose-I crystal structure. CNFs/CNPs composites behave as pseudoplastic fluids with shear-thinning properties.

Compared with pure CNFs, CNFs/CNPs composites possess smoother surface morphology. Their crystallinity index increases from 35.40 % to 45.38 %, and the temperature of maximum thermal-degradation rate rises from 361.33 °C to 376.40 °C. Composite formation with CNPs improves thermal stability, consistent with the rule that higher crystallinity corresponds to higher melting point.

CNFs/CNPs/PVA films exert antibacterial activity against *Escherichia coli*, *Staphylococcus aureus* and *Salmonella*. The antibacterial rates of CNFs/CNPs composites reach 95.04 % for *Staphylococcus aureus* and 93.92 % for *Escherichia coli*.

The as-synthesized CNFs/CNPs composites achieve enhanced thermal and antibacterial properties, showing application potential in coatings, packaging, medical supplies and antibacterial-material fields. Future work can further investigate their antibacterial mechanisms and expand biomedical applications by loading additional antibacterial chemical components.

References

[1] WANG J B, JIA N, WANG Z B, et al. Recent advances in porous materials made from tobacco waste[J]. Tobacco Science & Technology, 2020, 53(12): 96-105.
[2] LI C, WANG B, LI M Y, et al. Progress and prospects of research on resource utilization from tobacco organic waste[J]. Journal of Agro-Environment Science, 2024, 43(7): 1435-1448.
[3] LI J. Application effect of bio-organic fertilizer in the cultivation of flue-cured tobacco[J]. Modern Agricultural Science and Technology, 2016, 10: 170-175, 184.
[4] TIAN J L, LU Z, MA X Y, et al. The application of tobacco waste in fertilizer[J]. Agricultural Technology & Equipment, 2022(12): 69-75.
[5] YANG Y. Study on structure and combustion pyrolysis characteristics of tobacco cellulose[D]. Hefei: University of Science and Technology of China, 2018.
[6] de FRANCE K J, HOARE T, CRANSTON E D. Review of hydrogels and aerogels containing nanocellulose[J]. Chemistry of Materials, 2017, 29(11): 4609-4631.
[7] SHEN T H, DONG H, WANG P. Research progress on nanocellulose and its composite materials as orthopedic implant biomaterials[J]. Alexandria Engineering Journal, 2024, 87: 575-590.
[8] NICKERSON R F, HABRLE J A. Cellulose intercrystalline structure[J]. Industrial & Engineering Chemistry, 1947, 39(11): 1507-1512.
[9] AHOLA S, ÖSTERBERG M, LAINE J. Cellulose nanofibrils-adsorption with poly(amideamine)epichlorohydrin studied by QCM-D and application as a paper strength additive[J]. Cellulose, 2008, 15(2): 303-314.
[10] REN H W, XU Z H, XING X Y, et al. Research progress in the preparation, structural properties and application of nanocellulose[J]. Food Science, 2023, 44(17): 215-224.
[11] XIE H H, DU H S, YANG X H, et al. Recent strategies in preparation of cellulose nanocrystals and cellulose nanofibrils derived from raw cellulose materials[J]. International Journal of Polymer Science, 2018, 2018: 1-25.
[12] HUANG G H, LUO H Y, GUI R B, et al. Preparation and characterization of cellulose nanofibers by supercritical pretreatment-ball milling[J]. Transactions of China Pulp and Paper, 2022, 37(2): 9-14.
[13] LIU X L, WANG A, WANG C P, et al. Research progress in preparation and modification of cellulose nanofibril[J]. China Pulp & Paper, 2020, 39(4): 74-83.
[14] BAO H X, HU S H, HUANG Y, et al. Preparation and characterization of pineapple peel cellulose nanofibrils by dilute alkali-ball milling synergistic method[J]. Food and Fermentation Industries, 2023, 49(10): 64-70,77.

[15] MENG F J, HUANG H D, LIANG X Y, et al. Preparation and hydrophobicity of carbon nanofibers modified by nanocellulose[J]. New Chemical Materials, 2023, 51(6): 98-102,108.
[16] ZHANG F, TAO H R, MAO Y C, et al. Research progress on nanocellulose-based inorganic composite antiba cterial film materials[J]. Fine Chemicals, 2022, 39(6): 1081-1088.
[17] LIU Y, LI B L, GAO B S, et al. Fabrication and antioxidant properties of carvacrol/gelatin/polyvinyl alcohol fi brous membranes[J]. Fine Chemicals, 2023, 40(9): 1910-1918.
[18] MA J B, DAI J, LIAO T X, et al. Preparation and properties of lemon peel/polyvinyl alcohol/bacterial cellulo se composite membrane[J]. Food and Fermentation Industries, 2024, 50(15): 104-111.
[19] KANG X Y, DING Y H, BAI J Y, et al. Preparation and properties of nano-ZnO/cellulose nanocrystal/polyviny l alcohol composite films[J]. Plastics, 2023, 52(2): 6-9,55.
[20] WANG X B. Preparation and properties of cellulose based multifunctional composite films[D]. Xi'an: Shaan xi University of Science & Technology, 2022.
[21] LIU Y, BAI X M, CHEN M J, et al. Fabrication and visible-light-activated bacteriostasis of polyvinyl alcohol/ g-C_3N_4 composite nanofiber membranes[J]. Polymer Materials Science & Engineering, 2023, 39(2):71-79.
[22] LI Y Z, YU M J, HUI H, et al. Multiple factor analysis on preparation of cellulose nanofiber by ball milling fro m softwood pulp[J]. BioResources, 2018,13(2):2397-2410.
[23] ANNA S, SILVIJA K, JANIS G, et al. Nanofibre electrospinning poly(vinyl alcohol) and cellulose composite m ats obtained by use of a cylindrical electrode[J]. Advances in Materials Science and Engineering, 2013,201 3:1-6.
[24] LU Z H, ZHANG H, LIU L Q, et al. Study on cellulose nanofibers (CNF) distribution behaviors and their roles in improving paper property[J]. Industrial Crops Products, 2023,201:116897.
[25] DEVENDRAN T, SAITO Y, SHIMAMURA Y, et al. Investigation of physical and mechanical properties of nan o-pulverized cellulose nanofiber preform sheets for CNFs thermoset nanocomposites application[J]. Woo d Science and Technology, 2020,54(5):1-14.
[26] ZHANG H, DAI H J, CHEN Y, et al. Preparation and structure characterization of lemon seed cellulose nano fibrils using ionic liquid-assisted ball milling[J]. Food Science, 2021,42(7):120-127.
[27] YU W, WANG C Y, YI Y J, et al. Direct pretreatment of raw ramie fibers using an acidic deep eutectic solven t to produce cellulose nanofibrils in high purity[J]. Cellulose, 2020,28(1):1-14.
[28] SOFLA K R M, BROWN J R, TSUZUKI T, et al. A comparison of cellulose nanocrystals and cellulose nanofibr es extracted from bagasse using acid and ball milling methods[J]. Advances in Natural Sciences: Nanoscie nce and Nanotechnology, 2016,7(3):035004.
[29] HU W, ZHOU Y R, JIANG D L, et al. Nanochannel electrochemical sensor based on multi-walled carbon nan otubes and gold nanoparticles for heavy metal detection in grains[J]. Science and Technology of Food Ind ustry, 2025,46(15):324-333.
[30] WANG Q B. Preparation and characterization of cellulose nanofibrils and self-assembly nanopaper from t obacco stalk[D]. Kunming: Kunming University of Science and Technology, 2018.
[31] MENG D L, LIU B, ZOU L, et al. Preparation and characterization of cellulose nanocrystal from tobacco stra w[J]. Journal of Yunnan University (Natural Sciences Edition), 2021,43(2):343-351.
[32] DU P, XU Y J, LI W J, et al. Prepared and properties of high-permeability CNF/Ring-topologically CNC comp osite film[J]. China Pulp & Paper, 2023,42(5):37-42,125.
[33] WANG X Y. Fabrication and characterization of cellulose nanocrystal as well as cellulose nanofibril and the ir aerogels[D]. Nanjing: Nanjing Forestry University, 2018.
[34] DONG M L, SU W H, SHU X, et al. Preparation of multiscale lignocellulosic nanofibrils by p-toluenesulfonic acid hydrolysis and high-pressure homogenization[J]. Transactions of China Pulp and Paper, 2023,38(2):5 2-58.
[35] SUN X X, WU Q L, ZHANG J L, et al. Rheology, curing temperature and mechanical performance of oil well cement: Combined effect of cellulose nanofibers and graphene nano-platelets[J]. Materials & Design, 201 7,114:92-101.
[36] HE X F, GUO F Q, GE T J, et al. Study on rheological behavior and thermal stability of MC nylon/cellulose n anofibers composite[J]. Plastics Science and Technology, 2022,50(12):28-32.
[37] LYU T Y, ZHANG S M, CHEN Y, et al. Research progress on preparation methods of different morphologies of nanocellulose[J]. Food and Fermentation Industries, 2022,48(8):281-288.
[38] ZHOU J. Fabrication of strong and tough cellulose nanofibril films and their strengthening and toughening mechanism[D]. Guangzhou: South China University of Technology, 2022.

[39] LI X Q. Preparation and modification of nanocellulose and its application in waterborne coatings[D]. Beijing: China National Pulp and Paper Research Institute Co., Ltd., 2023.
[40] XIE M M, GAO M, YANG Y, et al. Antibacterial nanomaterials: Mechanisms, impacts on antimicrobial resistance and design principles[J]. Angewandte Chemie, 2023,135(17):1-25.
[41] DIAZ L D, MERCHÁN D M, PÉREZ P, et al. N-doped carbon nanoparticles as antibacterial agents on escherichia coli: The role of the size and chemical composition of nanoparticles[J]. Coatings, 2023,13(7):1169.
[42] ZHANG C, ZHANG L, LIU X H, et al. Research advances in antibacterial properties and applications in biomedicine of carbon nanomaterials[J]. Materials Reports, 2020,34(S1):53-57.
[43] CHEN L J, WANG H B, LI X, et al. Highly hydrophilic carbon nanoparticles: Uptake mechanism by mammalian and plant cells[J]. RSC Advances, 2018,8(61):35246-35256.